Available online at www.sciencedirect.com

SciVerse ScienceDirect

journal homepage: www.elsevier.com/locate/ijrefrig

Comparative analysis of low temperature industrial refrigeration systems

P. Mumanachit, D.T. Reindl, G.F. Nellis*

University of Wisconsin, 432 North Lake St, Madison, WI 53706, USA

ARTICLE INFO

Article history:
Received 20 March 2010
Received in revised form
5 September 2011
Accepted 23 February 2012
Available online 10 March 2012

Keywords:
Cascade system
Industrial freezer
Ammonia
Carbon dioxide
Optimization

ABSTRACT

This paper compares the energy performance and economics of a direct two-stage ammonia system to an ammonia–carbon dioxide cascade system for low temperature (below −40 °C) applications. Component and system models are developed for both the direct ammonia and the ammonia–carbon dioxide cascade options. These models provide the basis for quantifying the relative operating costs for both systems on annual and life-cycle bases.

The analysis shows that the ammonia–carbon dioxide cascade system option using a shell-and-tube cascade condenser offers the potential for increased energy efficiency when compared to a direct two-stage ammonia system when operating with evaporating temperatures that are below −46.2 °C. For the cascade system option, the analysis shows that a shell-and-tube cascade heat exchanger with design approach temperature of 5.6 °C provides the optimal balance of system performance with capital cost.

Analyse comparative de systèmes frigorifiques industriels à basse température

Mots clés : Systeme à cascade ; Congelateur industriel ; Ammoniac ; Dioxyde de carbone ; Optimisation

1. Introduction

The majority of industrial refrigeration systems operate using anhydrous ammonia (NH_3) as the refrigerant. Ammonia is a natural refrigerant that is environmentally-friendly with low global warming potential (GWP) and no ozone depletion potential (ODP), (UNEP, 2006; Calm and Hourahan, 2007)). However, the toxicity of ammonia to humans and its potential to contaminate products upon release have challenged practitioners to consider other refrigerant alternatives that may provide value by overcoming these drawbacks while maintaining or enhancing the overall performance of a refrigeration system. Another disadvantage of ammonia is related to its use in systems that require very low operating temperatures. Although the triple point of ammonia at −77.7 °C represents one constraint, another is the increase in compression equipment required as the ammonia suction pressures decrease. As the required evaporating temperature

* *Corresponding author*. Tel.: +1 608 262 6381; fax: +1 608 262 6209.
E-mail address: dreindl@wisc.edu (D.T. Reindl).
0140-7007/$ – see front matter © 2012 Elsevier Ltd and IIR. All rights reserved.
doi:10.1016/j.ijrefrig.2012.02.009

Nomenclature

a–f curve fit or regression coefficients
$ACC_{cascade}$ adjusted capital cost for the cascade system (the sum of the capital cost for the cascade heat exchanger and the compressors required for the two stages), $US
$ACC_{two\text{-}stage}$ adjusted capital cost for the two-stage system (the sum of the capital cost for the compressors for the two stages), $US
ACD adjusted capital cost difference (cascade − two-stage), $US
AR heat exchanger aspect ratio (shell diameter divided by shell length)
$\dot{C}_{min,condenser}$ minimum capacitance rate for the evaporative condenser, kW m^{-2}
$\dot{C}_{min,sh}$ minimum capacitance rate in the desuperheating section of the cascade condenser, kW m^{-2}
$c_{p,a}$ heat capacity at constant pressure for ambient air leaving the condenser, kJ kg^{-1} K^{-1}
$c_{p,CO_2,sh}$ heat capacity at constant pressure for carbon dioxide evaluated at the mean temperature of desuperheating fluid, kJ kg^{-1} K^{-1}
CAP manufacturer's-rated compressor capacity, kW
$CAP_{condenser}$ condenser heat rejection capacity, kW
CAP_{nom} nominal condenser heat rejection capacity, kW
CFM_{nom} nominal condenser volumetric air flow rate, ft^{-3} min^{-1}
$Cost_{booster}$ capital cost for the booster compressors in the two-stage system, $US
$Cost_{CHE}$ capital cost for the cascade heat exchanger, $US
$Cost_{intercooler}$ capital cost for the intercooler in the two-stage system, $US
$Cost_{recip}$ capital cost for a reciprocating compressor, $US
$Cost_{HPC}$ capital cost for a compressors in the high temperature circuit or high-stage of a two-stage system, $US
COP coefficient of performance representing the cooling capacity over work input
D_i inside diameter of heat exchanger tube, m
FC first or capital cost, $US
G_{CO_2} mass flux of condensing carbon dioxide, kg s^{-1} m^{-2}
$h_{a,o}$ Enthalpy of air at the condenser outlet, kJ kg^{-1}
$h_{a,i}$ Enthalpy of air at the condenser inlet, kJ kg^{-1}
$h_{a,TRS}$ enthalpy of air achieved leaving the condenser saturated at the refrigerant condensing temperature, kJ kg^{-1}
$\overline{h}_{CO_2,sat}$ average heat transfer coefficient on the carbon dioxide side of the cascade heat exchanger, kW m^{-2} K^{-1}
$\overline{h}_{NH_3,sat}$ average heat transfer coefficient on the ammonia-side of the cascade heat exchanger, kW m^{-2} K^{-1}
$\overline{h}_{CO_2,sh}$ average heat transfer coefficient of desuperheating carbon dioxide side in the cascade heat exchanger, kW m^{-2} K^{-1}
HRF condenser heat rejection factor (ratio of nominal to actual heat rejection capacity)
$k_{CO_2,L}$ thermal conductivity of carbon dioxide in the liquid phase, kW m^{-1} K^{-1}
$k_{CO_2,sh}$ thermal conductivity of vapor carbon dioxide desuperheating in the cascade condenser, kW m^{-1} K^{-1}
LCC life-cycle cost, $US
LCS life-cycle savings, $US
$\dot{m}_a$ mass flow rate of air entering the condenser, kg s^{-1}
$\dot{m}_{LTC}$ mass flow rate of desuperheating fluid in the low temperature circuit, kg s^{-1}
N_{comp} number of compressors in each refrigerating circuit
$\overline{Nu}_{CO_2,sat}$ average Nusselt number of carbon dioxide undergoing a phase change in the cascade heat exchanger
$\overline{Nu}_{CO_2,sh}$ average Nusselt number of the carbon dioxide side undergoing desuperheating in the cascade heat exchanger
$NTU_{cascade,sh}$ number of transfer units in the desuperheating portion of the cascade heat exchanger
$NTU_{condenser}$ number of transfer units for the condenser
OC annual operating cost, $US
$OC_{cascade}$ annual operating cost for the cascade system, $US
$OC_{two\text{-}stage}$ annual operating cost for the two-stage system, $US
P_1 multiplier to convert operating cost to the present value for life-cycle costing
P_{head} condensing pressure in the high temperature circuit
POW manufacturer's-rated compressor power, kW
$Pr_{CO_2,L}$ Prandtl number for saturated liquid carbon dioxide
$Pr_{CO_2,sh}$ Prandtl number for carbon dioxide vapor desuperheating in the cascade heat exchanger
$\dot{q}''_{cascade,sat}$ cascade heat exchanger heat flux, kW m^{-2}
$\dot{q}''_{cascade,sh}$ heat flux in the desuperheating section of the cascade heat exchanger, kW m^{-2}
$\dot{Q}_{condneser,net}$ condenser heat rejection capacity, kW
$\dot{Q}_{cascade,sat}$ cascade heat exchanger load, kW
$\dot{Q}_{cooling}$ design refrigeration load, kW
$\dot{Q}_{condenser,max}$ maximum condenser capacity achieved when the leaving air is saturated at the refrigerant condensing temperature, kW
$R_{CO_2,sat}$ thermal resistance of the condensing carbon dioxide side in the cascade heat exchanger, °C kW^{-1}
R_{CO_2SH} thermal resistance of the superheated carbon dioxide side in the cascade heat exchanger, °C kW^{-1}
$R_{NH_3,sat}$ thermal resistance of the evaporating ammonia in the cascade heat exchanger, °C kW^{-1}
$R_{tube,sat}$ thermal resistance due to conduction through the tube separating the carbon dioxide side from ammonia in the cascade heat exchanger, °C kW^{-1}
$\overline{Re}_{CO_2,sat}$ average Reynolds number for the carbon dioxide side of the cascade heat exchanger

$Re_{CO_2,sh}$	Reynolds number for vapor carbon dioxide desuperheating in the cascade heat exchanger
SDT	compressor saturated discharge temperature, °C
SST	compressor saturated suction temperature, °C
$STAR$	heat exchanger shell-to-tube area ratio (total cross-sectional area of the outer shell to that of the tube bundle)
$STLR$	heat exchanger shell-to-tube length ratio (ratio of the shell length to the length of one tube bundle pass)
$\overline{T}_{CO_2,sh}$	mean temperature of desuperheating carbon dioxide in the cascade heat exchanger, °C
Tc	ammonia temperature, °C
$T_{cascade}$	cascade condensing temperature, °C
$T_{CO_2,sh}$	discharge temperature of the superheated low temperature circuit refrigerant (carbon dioxide), °C
$T_{cond,sat}$	saturated temperature of condensing refrigerant in the high temperature circuit, °C
$T_{evap,sat,HTC}$	saturation temperature of evaporating refrigerant in the high temperature circuit, °C
T_{int}	saturation temperature of the intermediate pressure that optimizes the two-stage system, °C
T_{wb}	ambient wet-bulb temperature, °C
$UA_{condenser}$	overall conductance of the condenser, kW C^{-1}
$UA_{cascade,sat}$	overall conductance of the cascade heat exchanger at saturation conditions, kW C^{-1}
$UA_{cascade,sh}$	overall conductance in the desuperheating section of the cascade heat exchanger, kW C^{-1}

Greek symbols

γ	dimensionless constant (Eq. (10))
ΔFC	premium difference which represents the maximum additional capital cost for the system with higher efficiency for equal LCC for the lower efficiency system, $US
$\Delta T_{cascade}$	cascade heat exchanger approach temperature, K
$\varepsilon_{cascade,sh}$	effectiveness of the desuperheating portion of the cascade heat exchanger
$\varepsilon_{condenser}$	effectiveness of the condenser
$\rho_{CO_2,L}$	density of carbon dioxide in the liquid phase, kg m^{-3}
$\rho_{CO_2,vap}$	density of carbon dioxide in the vapor phase, kg m^{-3}
$\mu_{CO_2,L}$	dynamic viscosity of carbon dioxide in the liquid phase, kg m^{-1} s^{-1}

(and therefore pressure) decreases, the vapor-specific volume of ammonia increases significantly. The large specific volume at the compressor suction necessitates very large and costly compression equipment.

An alternative refrigeration system configuration for low temperature operation is the NH_3/CO_2 cascade refrigeration system. In this arrangement, carbon dioxide is maintained in a low temperature vapor compression circuit and coupled with an ammonia vapor compression refrigeration system through an indirect *cascade heat exchanger* (CHE). This arrangement separates both refrigerants so that each will operate in a desirable operating pressure/temperature range. In a cascade system, the desirable characteristic of high vapor density for the carbon dioxide at low temperatures can be leveraged with the desirable characteristics of ammonia at higher temperature (Taylor, 2002); however, the low-side for the carbon dioxide cascade arrangement is limited by the triple point of carbon dioxide, −56.6 °C. Environmentally, carbon dioxide is considered a natural refrigerant and is non-toxic and non-flammable with a GWP of 1 and an ODP of 0 (UNEP, 2006; Calm and Hourahan, 2007). A variation on the cascade arrangement involves the use of carbon dioxide as a volatile secondary fluid to heat exchange between loads and the ammonia system. In this case, the low temperature circuit is void of a compressor.

There has recently been a renewed interest in cascade refrigeration systems using NH_3/CO_2 as an alternative to the conventional two-stage direct ammonia system (Page, 2002; Pearson, 2005). Within the U.S., several cascade systems have recently been installed in applications ranging from supermarket systems to large food production and distribution storage warehouses. For example, Nestlé USA has installed cascade systems in their Jonesboro, AR and Mount Sterling, KY facilities. US Cold Storage has installed ammonia–cascade systems in their distribution warehouses located in Bethlehem, PA; Lebanon, IN; and Fresno, CA. Internationally, there has been considerable activity involving the field installations of ammonia–carbon dioxide cascade systems. For example, Nestlé has installed a large ammonia–carbon dioxide cascade system in a freeze-drying plant located in the UK (Homsy, 2003).

Dopazo et al. (2007) developed a mathematical model of the cascade system that focuses on maximizing the system operating efficiency by evaluating the impact associated with changes in several of the operating parameters. The parameters that were examined included the evaporating temperature, the condensing temperatures of each refrigerant, the compressor isentropic efficiency, and the approach temperature at the cascade heat exchanger. Getu and Bansal (2008) performed a similar analysis by constructing a thermodynamic model to carry out a multi-linear regression analysis of the operating parameters in order to optimize the operating performance of the cascade system. Lee et al. (2006) analyzed the cascade system using a thermodynamic model in order to determine the optimal condensing temperature of carbon dioxide in the cascade heat exchanger over a range of operating conditions. Lee et al. also integrated compressor efficiency correlations from actual compressors. These studies only focused on optimizing the *COP* of the cascade system and never compared the performance of the cascade system to a multi-stage ammonia system.

Other comparative studies between the two system configurations have suggested that NH_3/CO_2 cascade systems result in lower efficiency (higher energy consumption) throughout the range of temperatures that are typically encountered in food freezing and storage applications. Pillis (2009) conducted an energy analysis of both CO_2 and NH_3 compressors in the low temperature circuit of cascade

and multi-stage systems, respectively, and reported that CO_2 compressors have higher energy consumption while operating at suction temperatures ranging from −28.9 °C to −51.1 °C compared to ammonia compressors. The improved operating efficiencies for carbon dioxide reciprocating compressors claimed by manufacturers still resulted in a higher energy penalty compared to the screw compressors used for ammonia. Ouadha et al. (2007) presented an efficiency comparison after maximizing the exergy of the cycles. The results indicated that carbon dioxide has the advantage of allowing the cascade system to utilize smaller compression equipment but that the second law efficiency of the cascade cycle is lower than the two-stage system.

A detailed analysis and optimization based on an economic comparison of the life-cycle savings associated with a cascade refrigeration system using a long-term system performance simulation has not previously been reported in the literature. In this paper, we present a quantitative comparison of a NH_3/CO_2 cascade system with a conventional two-stage direct ammonia system under identical operating conditions (Mumanachit, 2009). An analysis using component-based system-level performance simulations is carried out for hourly intervals over a 20-year life-cycle. Both systems are specified to meet a 2392 kW thermal load over a range of evaporating temperatures below −40 °C.

2. Cycle descriptions

Fig. 1 shows a simple schematic of a two-stage system using ammonia. Saturated ammonia vapor leaves the low temperature evaporator after absorbing heat from the load and is compressed to an intermediate pressure by one or more booster compressors. The superheated vapor leaving the booster compressors is de-superheated in an intermediate pressure vessel (the intercooler). Saturated intermediate pressure vapor is then drawn into one or more high-stage compressors where it is compressed a pressure sufficiently high to reject heat from the system to the outdoor environment through the condenser.

Fig. 2 shows a diagram of a cascade refrigeration system using CO_2 in the low temperature circuit (LTC) and NH_3 in the high temperature circuit (HTC). The heat load absorbed into the LTC is transferred to the HTC through an indirect heat exchange process using a cascade heat exchanger in order to avoid physically mixing the two refrigerant streams.

3. System component models

The operating characteristics associated with each cycle configuration are determined from a thermodynamic analysis of the underlying processes and the refrigerant thermophysical properties at each cycle state point. Each component model is developed by incorporating performance data from appropriate equipment specified based on the system requirements. The system-level model integrates these detailed component models and therefore provides a framework with which to perform meaningful economic comparisons of the two system configurations.

Three components are common to both configurations: compressors, evaporative condensers, and evaporators. Two system components are unique to each system: the intercooler (for the two-stage system) and the cascade heat exchanger (for the cascade system). An intercooler is simply a storage vessel that physically couples the two circuits in the multi-stage system and also acts as both a de-superheater and a liquid–vapor separator. The cascade heat exchanger is an essential piece of equipment in the cascade system; however,

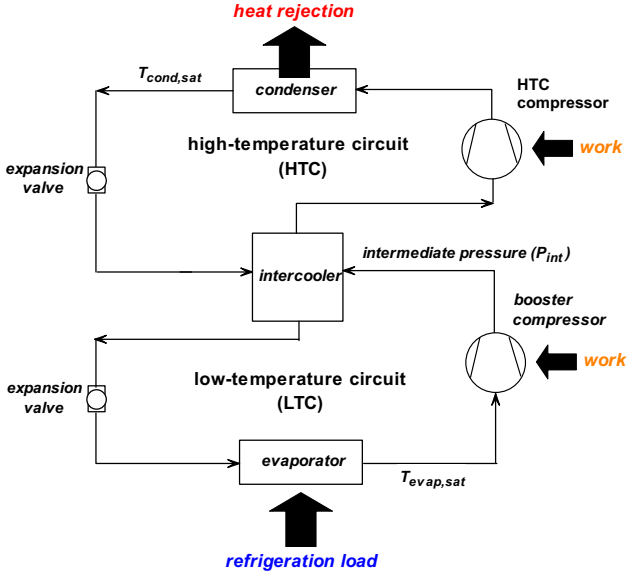

Fig. 1 – Schematic diagram of an intercooled two-stage vapor compression cycle.

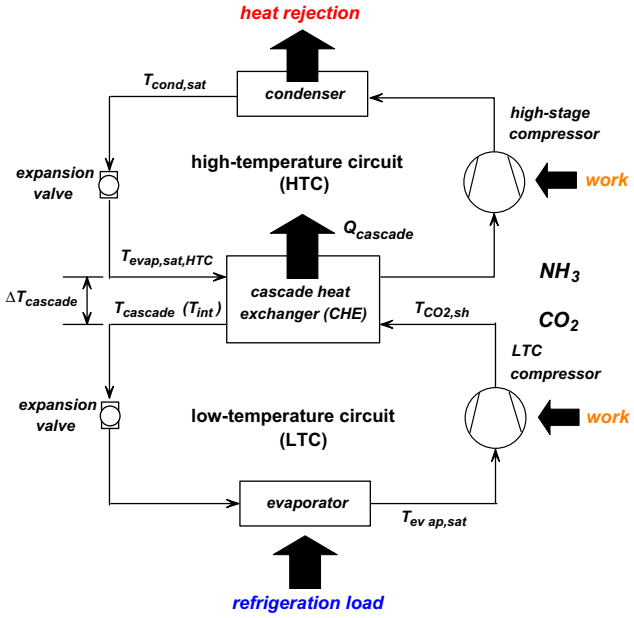

Fig. 2 – Schematic diagram of a cascade vapor compression refrigeration cycle.

its thermal performance and cost significantly impact the efficiency and capital cost of the system.

4. Compressor model

The compressors installed in a refrigeration system using carbon dioxide or other refrigerants with low vapor-specific volume (high vapor density) can be either reciprocating or screw compressors. For the purpose of simulating the performance of the compressors used in both the ammonia and the carbon dioxide circuits, appropriate data from compressor manufacturers are employed (JCI, 2010 and Grasso, 2008). The compressor type, displacement, and operating temperature range selected for use in each system are listed in Table 1. Note that the same twin screw compressor is used for the high temperature compressor (HTC) for both systems. In the cascade system, a reciprocating compressor is selected for use in the low temperature carbon dioxide circuit. In the two-stage ammonia system, a twin screw compressor is selected for the low temperature (booster) compressor.

The full-load capacity (*CAP*) reported by the manufacturer for each compressor is curve fit as a function of the saturated suction temperature (*SST*) and saturated discharge temperature (*SDT*) using a bi-quadratic function:

$$CAP = a + b\,SST + c\,SST^2 + d\,SDT + e\,SDT^2 + f\,SST\,SDT \quad (1)$$

The compressor power at full-load (*POW*) is curve fit in a similar manner:

$$POW = a + b\,SST + c\,SST^2 + d\,SDT + e\,SDT^2 + f\,SST\,SDT \quad (2)$$

Coefficients for the bi-quadratic functions given in Eqs. (1) and (2), can be found in Mumanachit (2009).

To meet the peak refrigeration loads in a plant, multiple compressors are often required. In determining the number of compressors required in each circuit, the design cooling load is divided by the compressor full-load capacity operating at its design suction and discharge pressures.

$$N_{comp} = \frac{\dot{Q}_{cooling}}{CAP} \quad (3)$$

The design cooling load in the low temperature circuit is the same for both systems, but the high temperature circuit load is dependent on the intermediate condition and the efficiency of the low temperature compressors. The number of compressors calculated using Eq. (3) is rounded up to the next integer so that the aggregate capacity of the operating compressors is able to meet the required load. Any excess compressor capacity is reduced by running a single compressor at part-load with the remaining compressors operating at full-load. The efficiency of a screw compressor diminishes non-linearly as the machine unloads. Manufacturer's data are used to characterize the operating efficiency of the screw compressor at part-load conditions as summarized by Mumanachit (2009). The part-load performance for reciprocating compressors is assumed near-linear (Manske, 1999).

5. Cascade heat exchanger model

The LTC compressor discharges superheated CO_2 to the cascade heat exchanger (CHE) where it is desuperheated and liquefied as it transfers heat to lower temperature evaporating ammonia in the HTC. The CHE is assumed to be a shell-and-tube heat exchanger, as shown in Fig. 3. Carbon dioxide condenses to a saturated liquid on the tube-side of the heat exchanger while ammonia evaporates to a saturated vapor on the shell-side in a flooded configuration. The CHE is modeled by separating the sensible energy change process (desuperheating) on the CO_2 side from the latent energy change process (condensing). The design size and operating conditions associated with the cascade system are based on an actual heat exchanger that is installed in an operating cascade refrigeration system at a plant located in the central U.S. All design parameters used to develop the cascade heat exchanger model are summarized in Table 2.

The aspect ratio (*AR*) of the heat exchanger is the ratio of the outer shell diameter to the shell length. The shell-to-tube area ratio (*STAR*) is the ratio of the total cross-sectional area of the outer shell to that of the tube bundle and the shell-to-tube length ratio (*STLR*) is the ratio of the shell length to the length of one tube bundle pass. These three parameters are fixed as the cascade heat exchanger size is adjusted in subsequent analyses. As the cascade heat exchanger size (i.e. number of tubes, shell diameter, length and etc.) varies with the approach temperature, the physical dimensions of the heat exchanger vary accordingly.

5.1. *Cascade heat exchanger condensing section*

In the condensing section of the CHE, both fluid streams undergo isothermal heat exchange thus the approach temperature ($\Delta T_{cascade}$) between these two streams dictates the required conductance ($UA_{cascade,sat}$).

$$\dot{Q}_{cascade,sat} = UA_{cascade,sat}\Delta T_{cascade} \quad (4)$$

The conductance of the condensing section is given by:

Table 1 – Summary of compressor types and performance characteristics.

Type	Displacement [$m^3\,h^{-1}$]	System/Stage	Saturation temperature, [°C]	
			Suction	Discharge
Twin screw	1770	Both systems/high stage, HTC	−20.6 to −6.7	23.9 to 40.6
Twin screw	6765	Two-stage booster	−51.1 to −28.9	−17.8 to −1.1
Reciprocating	167	Cascade/LTC	−51.1 to −37.2	−17.8 to −9.4

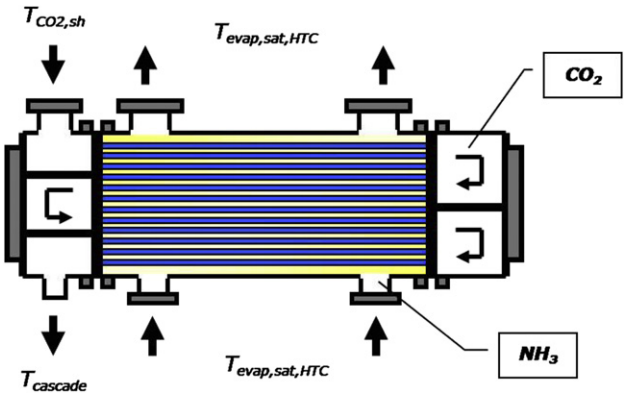

Fig. 3 – Schematic diagram of a 4-pass, shell-and-tube cascade heat exchanger.

$$UA_{cascade,sat} = \frac{1}{R_{CO_2,sat} + R_{tube,sat} + R_{NH_3,sat}} \tag{5}$$

where $R_{CO_2,sat}$, $R_{tube,sat}$ and $R_{NH_3,sat}$ are the thermal resistance to convection between the condensing carbon dioxide and the inner tube surface, the resistance to conduction across the tube thickness, and the resistance to convection between outside tube surface and evaporating ammonia, respectively. The convective heat transfer coefficient on the CO_2 side ($\overline{h}_{CO_2,sat}$), is given by:

$$\overline{h}_{CO_2,sat} = \frac{\overline{Nu}_{CO_2,sat} k_{CO_2,L}}{D_i} \tag{6}$$

where $k_{CO_2,L}$ is the thermal conductivity of carbon dioxide in the liquid phase and $\overline{Nu}_{CO_2,sat}$ is the average Nusselt number which is estimated using a correlation proposed by Calvallini et al. (2002).

$$\overline{Nu}_{CO_2,sat} = 0.05\, \overline{Re}^{0.8}_{CO_2,sat} Pr^{1/3}_{CO_2,L} \tag{7}$$

Table 2 – Design operating conditions and geometry of the cascade heat exchanger.

Parameter	Description	Values
$T_{cond,sat}$	Saturated condensing temperature of NH_3	35 °C
$T_{cascade}$	Saturated condensing temperature of CO_2	−15 °C
$T_{evap,sat}$	Saturated evaporating temperature of CO_2	−40 °C
$\Delta T_{cascade}$	Cascade heat exchanger approach temperature	5.6 °C
$\dot{Q}_{cascade}$	Design cascade heat exchanger heat load	2835 kW
D_o	Outer tube diameter	1.588×10^{-2} m
D_i	Inner tube diameter	1.34×10^{-2} m
th_{tube}	Tube wall thickness	1.245×10^{-3} m
AR	Aspect ratio	0.1303
STAR	Shell-to-tube area ratio	2.381
STLR	Shell-to-tube length ratio	1.707
N_{pass}	Number of tube passes	4

where $Pr_{CO_2,L}$ is the Prandtl number of saturated liquid CO_2 and $\overline{Re}_{CO_2,sat}$ is an average Reynolds number, determined by averaging the equivalent Reynolds number over the range of quality encountered in the heat exchanger as presented by Cavallini et al. (2002). The equivalent Reynolds number is simplified for the computation of the heat transfer coefficient of carbon dioxide during the condensation process according to:

$$\overline{Re}_{CO_2,sat} = \frac{G_{CO_2} D_i}{2\mu_{CO_2,L}} \left(\left(\frac{\rho_{CO_2,L}}{\rho_{CO_2,vap}} \right)^{0.5} + 1 \right) \tag{8}$$

where $\mu_{CO_2,L}$ is the dynamic viscosity of the refrigerant in the liquid phase, and $\rho_{CO_2,L}$ and $\rho_{CO_2,vap}$ are the refrigerant density in the liquid and vapor phase, respectively. G_{CO_2} is the mass flux of condensing carbon dioxide.

The convective heat transfer coefficient of evaporating ammonia is calculated as a function of the heat flux ($\dot{q}''_{cascade,sat}$) using a correlation proposed by Ayub (2004),

$$\overline{h}_{NH_3,sat} = \gamma \left(\dot{q}''_{cascade,sat} \right)^{0.55} \tag{9}$$

where γ is a dimensionless constant that is defined as a function of the saturated evaporating temperature of ammonia (T_C):

$$\gamma = 0.291[-] + 3.9 \times 10^{-3} \left[\frac{1}{^oC} \right] T_C + 4.75 \times 10^{-4} \left[\frac{1}{^oC^2} \right] T_C^2 + 1.84 \times 10^{-5} \left[\frac{1}{^oC^3} \right] T_C^3 + 1.97 \times 10^{-7} \left[\frac{1}{^oC^4} \right] T_C^4 \tag{10}$$

5.2. CHE desuperheating section

An effectiveness-NTU method is used to model the desuperheating section of the CHE. This is appropriate because the specific heat capacity of carbon dioxide vapor is nearly constant while the capacitance rate of the ammonia evaporating on the shell-side of the tube bundle is, effectively, infinite. The number of transfer units in the desuperheating section ($NTU_{cascade,sh}$) for a heat exchanger where one fluid stream has an infinitely large capacitance rate is given by Nellis and Klein (2009) as,

$$NTU_{cascade,sh} = -\ln\left(1 - \varepsilon_{cascade,sh}\right) \tag{11}$$

where the effectiveness of the desuperheating section ($\varepsilon_{cascade,sh}$) is calculated as,

$$\varepsilon_{cascade,sh} = \frac{T_{CO_2,sh} - T_{cascade}}{T_{CO_2,sh} - T_{evap,sat,HTC}} \tag{12}$$

$T_{CO_2,sh}$ is the discharge temperature of superheated LTC refrigerant, $T_{cascade}$ is the cascade condensing temperature, and $T_{evap,sat,HTC}$ is the saturated evaporating temperature of HTC refrigerant. The required conductance rate of the desuperheating section, $UA_{cascade,sh}$, is calculated from the number of transfer units, $NTU_{cascade,sh}$, and the minimum refrigerant capacitance rate, $\dot{C}_{min,sh}$, according to:

$$UA_{cascade,sh} = NTU_{cascade,sh} \dot{C}_{min,sh} \tag{13}$$

The minimum capacitance rate in the desuperheating section ($\dot{C}_{min,sh}$) is always on the CO_2 side,

$$\dot{C}_{min,sh} = \dot{m}_{LTC} c_{p,CO_2,sh} \quad (14)$$

where $\dot{m}_{LTC}$ is the mass flow rate of the desuperheating refrigerant and $c_{p,CO_2,sh}$ is the specific heat capacity of carbon dioxide vapor; the value of $c_{p,CO_2,sh}$ is evaluated at a mean temperature of the desuperheating refrigerant ($\overline{T}_{CO_2,sh}$). The conductance of the desuperheating section is the inverse of the sum of the resistances between the two refrigerant streams,

$$UA_{cascade,sh} = \frac{1}{R_{CO_2,sh} + R_{tube,sh} + R_{NH_3,sh}} \quad (15)$$

where $R_{CO_2,sh}$, $R_{tube,sh}$ and $R_{NH_3,sat}$ are the thermal resistance to convection between desuperheating CO_2 and the inner tube surface, the resistance to conduction through the tube walls and the resistance to convection between boiling ammonia on the shell-side and the outer tube surface, respectively.

The heat transfer coefficient of the single-phase CO_2 ($\overline{h}_{CO_2,sh}$) is calculated according to,

$$\overline{h}_{CO_2,sh} = \frac{\overline{Nu}_{CO_2,sh} k_{CO_2,sh}}{D_i} \quad (16)$$

where $k_{CO_2,sh}$ is the thermal conductivity of the desuperheating carbon dioxide. The Nusselt number, $\overline{Nu}_{CO_2,sh}$, is estimated using the Dittus-Boelter equation as presented in Incropera and DeWitt (2002),

$$\overline{Nu}_{CO_2,sh} = 0.023 Re^{4/5}_{CO_2,sh} Pr^{0.3}_{CO_2,sh} \quad (17)$$

where $Pr_{CO_2,sh}$ and $Re_{CO_2,sh}$ are the Prandtl number and the Reynolds number of desuperheating carbon dioxide, respectively. The thermal resistance, $R_{NH_3,sh}$, is inversely proportional to the convective heat transfer coefficient associated with boiling ammonia ($\overline{h}_{NH_3,sh}$), which is calculated using the same correlation described in the condensing section. Notice that the heat flux on the desuperheating section ($\dot{q}''_{cascade,sh}$) will be different from the heat flux in the condensing section and therefore the condensation heat transfer coefficient on the ammonia-side will be different in the two sections.

6. Evaporative condenser model

An evaporative condenser operates with superheated refrigerant entering through the top row of a serpentine configured condenser coil while cooling water, pumped from the water sump, is sprayed over the outside surface of tubes carrying condensing refrigerant. Condenser fans draw in ambient air that flows through the condenser coil in a counter-cross flow manner and picks up evaporating water as it absorbs both latent and sensible heat from the refrigerant stream. The moist air stream exits the top of the evaporative condenser in nearly a saturated condition at higher temperature. The amount of water vapor that can be absorbed by the ambient air depends on the ambient air wet-bulb temperature. Therefore, the ambient air wet-bulb temperature dictates the heat rejection capacity of the evaporative condensers. Fig. 4 shows a schematic diagram of an induced draft evaporative condenser modeled as part of the present systems analysis.

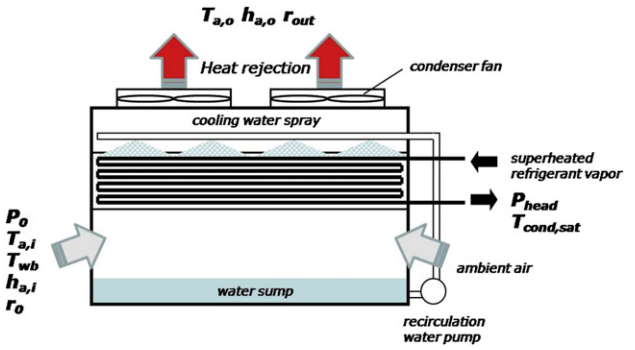

Fig. 4 – Schematic diagram of an air-drawn evaporative condenser.

The evaporative condenser model is based on manufacturer's condenser performance data (Evapco, 2005) for an induced draft air flow arrangement. These data are used to ascertain the effective thermal conductance of the condenser as a function of its operating condition with a semi-empirical model that is robust and realistic. The condenser nominal heat rejection capacity (CAP_{nom}), the nominal volumetric air flow (CFM_{nom}), and the heat rejection factor (HRF) are provided by the manufacturer. The available heat rejection capacity ($CAP_{condenser}$) of the condenser is determined by dividing the nominal heat rejection capacity by the heat rejection factor:

$$CAP_{condenser} = \frac{CAP_{nom}}{HRF} \quad (18)$$

The operating characteristics of the condenser are summarized in Table 3 and the design conditions used to carry out this analysis summarized in Table 4.

Because ammonia is condensing inside the condenser tube bundle with a large heat transfer coefficient, the air-side of the evaporative condenser limits the heat exchange process. There is an effectiveness associated with the heat rejection process and the effectiveness must account for both sensible and latent energy transfer. An enthalpy-based effectiveness approach presented by Manske (1999) is used to characterize the performance of evaporative condensers with good results. The enthalpy-based effectiveness of the evaporative condenser is defined as the ratio of the actual heat rejection to the maximum heat rejection by the condenser,

Table 3 – Evaporative condenser nominal operating characteristics.

Parameter	Description	Values
CAP_{nom}	Nominal heat rejection capacity given at 21.1 °C wet-bulb and 32.2 °C condensing temperature	2093 kW
CFM_{nom}	Nominal air flow rate	40 $m^3\ s^{-1}$
$Power_{fan}$	Condenser fan power at nominal condition	7.46 kW
N_{fan}	Number of fans	2

Table 4 – Design operating conditions for the evaporative condenser analysis.

Parameter	Description	Values
T_{wb}	Ambient air wet-bulb temperature	25 °C
$T_{cond,sat}$	Saturated condensing temperature of NH_3	35 °C
P_0	Atmospheric pressure	101.3 kPa
r_0	Ambient air relative humidity	60%
r_{out}	Relative humidity at outlet condition	100%
$\dot{Q}_{LTC}$	Low temperature circuit heat load	2391 kW
$\dot{Q}_{HTC}$	High temperature circuit heat load	3011 kW
$\dot{Q}_C$	Required system heat rejection	3747 kW

$$\epsilon_{condenser} = \frac{CAP_{condenser}}{\dot{Q}_{condenser,max}} = \frac{h_{a,o} - h_{a,i}}{h_{a,o,TRS} - h_{a,i}} \quad (19)$$

where $h_{a,i}$ is the specific enthalpy of the air stream at the condenser inlet corresponding to psychrometric state at the condenser inlet. The actual rate of heat rejection or the available capacity of the condenser ($CAP_{condenser}$) is proportional to the change in enthalpy of air from $h_{a,i}$ to $h_{a,o}$, which is the specific enthalpy of the outlet air leaving the condenser saturated at an outlet air condition. The maximum rate of heat rejected by the condenser ($\dot{Q}_{condenser,max}$) occurs when the air–water mixture undergoes its maximum possible enthalpy change. The maximum enthalpy of the outlet air ($h_{a,o,TRS}$) occurs if the air leaves the condenser saturated at the refrigerant condensing temperature.

Because one fluid stream (the ammonia) possesses an infinite capacitance rate, the effectiveness-NTU relation is provided by Nellis and Klein (2009) as,

$$NTU_{condenser} = -\ln(1 - \epsilon_{condenser}) \quad (20)$$

The minimum capacitance rate ($\dot{C}_{min,condenser}$) of the evaporative condenser is then

$$\dot{C}_{min,condenser} = \dot{m}_a c_{p,a} \quad (21)$$

where $c_{p,a}$ is the specific heat capacity of air leaving the condenser. The conductance of the condenser ($UA_{condenser}$) is calculated from,

$$UA_{condenser} = \dot{C}_{min,condenser} NTU_{condenser} \quad (22)$$

The conductance of the condenser is computed using the technique described above for each of the off-design conditions provided by the manufacturer and these results are correlated as a function of both T_{wb} and $T_{cond,sat}$.

$$UA_{condenser} = a + b \cdot T_{cond,sat} + c \cdot T_{wb} \quad (23)$$

The evaporative condenser is represented in the system model by Eq. (23). The condenser conductance is computed at any arbitrary operating condition. The conductance allows the calculation of the number of transfer units using Eq. (22) where the minimum capacitance rate is calculated from the air flow rate and inlet air temperature. The effectiveness is calculated from the number of transfer units using Eq. (20). The condenser heat rejection capacity ($\dot{Q}_{condenser,act}$) is predicted from the effectiveness according to Eq. (19).

7. System-level model and baseline system simulation

The component models are integrated in order to arrive at a complete and detailed system model that can be used to simulate energy performance and cost of operation. To ensure consistency in the performance simulation for both system configurations (two-stage and cascade), a common baseline of operation is defined in this section. The results of these simulations are later used in the life-cycle cost analysis in order to identify the more attractive system from an economic standpoint. The operating cost for each system, which is required for the economic analysis, is obtained by performing hourly analysis for an entire year. The energy use for each system is estimated using the hourly typical meteorological year (TMY) weather data (NREL, 2008) as a "forcing function" for the heat rejection of the system. Essential simulation criteria are summarized in Table 5.

In the present analysis, both the two-stage and cascade systems are characterized by an intermediate temperature that is a free parameter. The value of the intermediate temperature at which either the cascade heat exchanger or intercooler operates is allowed to vary in order to maximize the system efficiency. The optimization approach utilized used here maximizes the system COP over a range of head pressures and evaporating temperatures. The results of the optimization are the optimal intermediate pressure at the intercooler (for the two-stage configuration) and saturated condensing temperature of the carbon dioxide in the tube-side of the cascade heat exchanger (for the cascade configuration) evaluated over a matrix of condensing and evaporating conditions. These results are curve fit using a bi-quadratic regression with a 2nd order polynomial fit. Eq. (24) provides a functional representation for the optimal intermediate temperature of the cascade system as a function of the evaporating saturation temperature ($T_{evap,sat,HTC}$) and system head pressure (P_{head}),

$$T_{int} = a + b \cdot T_{evap,sat,HTC} + c \cdot T_{evap,sat,HTC}^2 + d \cdot P_{head} + d \cdot P_{head}^2 + f \cdot T_{evap,sat,HTC} \cdot P_{head} \quad (24)$$

The coefficients are determined based on a parametric analysis over a range of evaporating saturation

Table 5 – 12-month simulation input parameters and system model assumptions.

Parameters	Descriptions
Input parameters	Ambient air condition (TMY weather data)
Locations (U.S.)	Miami, FL, Madison, WI, Los Angeles, CA, Houston, TX
Modes of operation	• 8 h/day (2920 h yr^{-1}) and • 10 h/day (3650 h yr^{-1})
Head pressure	Variable based on weather but with a 930.8 kPa minimum
Evaporator heat load	2392 kW (constant)
Evaporating temperatures	−40 °C to −53.9 °C in 2.8 K steps

temperatures and system head pressures (Mumanachit, 2009). This approach allows the optimization, which is computationally time consuming and must be accomplished for every hour of operation, to be carried out only once. The identification of the optimal intermediate condition for any subsequent simulation can be obtained using Eq. (24).

Actual systems often have their intermediate temperature or pressure level dictated by requirements of intermediate temperature loads. Although optimizing the intermediate temperature is not entirely reflective of actual system operations, it represents a best case scenario for both the two-stage compression and cascade system operations.

8. Comparative analysis of system performance and economics

A consistent economic comparison of the multi-stage ammonia system with the NH_3/CO_2 cascade system configurations is accomplished by performing a life-cycle cost (LCC) analysis. The LCC analysis accounts for the total cost (capital and operating) associated with owning and operating a system throughout its lifetime. The LCC incorporates the net present value of all future operating (energy) costs for each system and the initial system capital cost.

$$LCC = P_1 \cdot OC + FC \tag{25}$$

where P_1 the conversion of life-cycle operating cost to the present value, OC is the annual operating cost, and FC the system capital cost. The main factors that effect P_1 are the fuel inflation rate (assumed to be 5.5%) and the discount rate (assumed to be 5.5%). The period of analysis considered is 20 years. Additional details on how sensitivity of economic factors influences the results can found in Mumanachit (2009).

The LCC for each system can be compared in order to determine the more economically attractive alternative by evaluating the life-cycle savings (i.e., the difference in life-cycle cost for the two system options). The operating cost of each system is determined explicitly using the 12-month simulation together with a limited set of economic parameters that are related to the present worth of the future cost of energy. For the purpose of an unambiguous comparison, it is possible to use these operating costs to calculate the difference in the first costs that will lead to both systems having an equal life-cycle cost. We define the *premium difference* as the maximum added capital cost that could be expended on the system with higher efficiency (i.e., the one with a lower operating cost) without exceeding the life-cycle cost of the less efficient system. The *premium difference* (ΔFC) is determined by applying the life-cycle cost equation, Eq. (25), to each system and setting them equal:

$$\Delta FC = P_1\left(OC_{cascade} - OC_{compound}\right) \tag{26}$$

where $OC_{cascade}$ and $OC_{two\text{-}stage}$ are first-year operating cost of the cascade and the two-stage systems, respectively. If ΔDFC is positive, the operating cost for the two-stage system is less and additional capital cost up to ΔFC could be expended without incurring a greater life-cycle cost than the cascade system option.

In order to evaluate the economic feasibility of each system, it is also instructive to estimate the capital cost of the system components that are associated with each system. The objective of this study is to investigate the difference in capital costs associated with implementing the cascade as opposed to the two-stage system. This is accomplished by estimating the cost of the major system components that differ between the two cycles. The major hardware cost associated with a cascade system that is not present with the two-stage system is the cascade heat exchanger. The major hardware cost associated with the two-stage system that is not present with the cascade system is associated with the very large compressors that are required to handle the high specific volume ammonia refrigerant at low temperature as well as the intercooler. Capital costs associated with piping for the two system options will also differ; however unlike compressors, vessels, and heat exchangers, capital cost estimates of piping are very installation specific. The carbon dioxide portions of the cascade system will require smaller pipe sizes but higher design pressures compared to the low-side of the two-stage ammonia system option. High-side piping for both system options will be substantially similar. As a result, piping costs are not included in the present economic analysis.

The adjusted capital cost of the cascade cycle is defined as the sum of the capital cost for the cascade heat exchanger and the compressors required for the two stages,

$$ACC_{cascade} = Cost_{CHE} + Cost_{RECIP} + Cost_{HPC} \tag{27}$$

The evaporators, condensers, etc. are common to both systems and therefore the cost of these components is not considered in the adjusted capital cost of either system. The adjusted capital cost of the two-stage system is the sum of the cost of the compressors for the two stages and the intercooler,

$$ACC_{two-stage} = Cost_{booster} + Cost_{HPC} + Cost_{intercooler} \tag{28}$$

The compressor cost is estimated using a correlation that relates cost to the suction volumetric flow rate of refrigerant vapor that is displaced by the compressors (JCI, 2010). The cost per flow is provided as a function of the flow rate and has been adjusted so that it includes the various overhead costs that are related to installation. Intercooler costs are obtained from a vessel manufacturer for the two-stage system. The vessel is sized to accommodate the total booster heat rejection with no additional intermediate temperature loads (JCI, 2010). The total cost of a CHE ($Cost_{CHE}$) includes the cost of the outer shell and the cost of the tube bundle. Capital costs for heat exchangers estimated using this technique do not include installation cost. Predictive correlations were developed by Lachner (2004) based on cost data obtained from an industry survey.

The adjusted capital difference (ACD) is the difference between the capital cost of the two options and corresponds to a life-cycle savings that is related to capital cost (in the same way that the premium difference corresponds to a life-cycle savings associated with operating cost). The ACD is defined with respect to the cascade system to be consistent with the definition of the premium difference.

$$ACD = ACC_{cascade} = ACC_{two-stage} \quad (29)$$

By considering the life-cycle cost difference associated with the capital cost difference and the operating energy cost difference associated with the two cycles, it is possible to establish the total life-cycle cost savings and therefore the evaporating temperature that will result in a true economic break-even cost. Since capital cost and operating cost each contributes to the total life-cycle cost of a system, the sum of the adjusted capital difference (*ACD*) and the premium difference (ΔFC) is the total life-cycle cost savings (*LCS*). The value of the total life-cycle cost savings is defined as,

$$LCS = ACD + \Delta FC \quad (30)$$

9. Results and discussion

9.1. System performance comparison

At low evaporating temperatures, one of the disadvantages of the two-stage system is that ammonia has a high vapor-specific volume. As a result, the performance of the two-stage system tends to degrade more rapidly than the cascade system at lower suction pressures due the rapid decline in the booster compressor's mass flow coupled with its decreasing volumetric efficiency. On the other hand, ammonia system tends to be more efficient at high evaporating temperatures.

Fig. 5 shows variation in operating efficiency (COP) as a function of evaporating temperature for the two configurations at three fixed values of head pressure: 931 kPa, 1103 kPa, and 1310 kPa. The ammonia two-stage system has higher system efficiency at higher evaporating temperatures while the cascade system is more efficient at lower evaporating temperatures. For each condensing temperature, there is a corresponding evaporating temperature where the *COP* for both systems is equal. For evaporating temperatures above −47.2 °C, the two-stage system has an increasing efficiency advantage over the cascade option.

Simulation of each system option over a 12-month period allows estimates of the electrical energy usage associated with each system to be developed which forms the basis for quantifying the operating cost and the associated savings of each option. Figs. 6 and 7 illustrate the annual energy usage of the cascade system as a function of evaporating temperature at each plant location for 8-h and 10-h day operating modes, respectively.

The climatic condition at each U.S. geographical location has an influence on system performance. The hot and humid conditions in Miami are associated with the highest average wet-bulb temperature among all four locations considered. Thus, a system operating in Miami will have a high required head pressure in order to reject heat to the surroundings and Miami has the highest annual energy usage. Houston has the next highest wet-bulb temperature and it follows Miami in a location-based energy usage trend but precedes Los Angeles and Madison, respectively.

The two-stage system has a higher *COP* at higher evaporating temperatures; this trend is also reflected in the annual energy usage. In order to clearly show this behavior, the annual energy usage in Houston as a function of evaporating temperature is shown in Fig. 8 for both the cascade and the two-stage system.

9.2. Operating cost savings

Using the estimated capital costs with the annual operating energy costs predicted by the 12-month simulation, an operating cost comparison between the cascade system and the two-stage system is developed. The premium difference, the operating cost savings defined with respect to the cascade system, is analyzed to quantify the operating cost savings. Figs. 9 and 10 present the premium difference at each location as a function of evaporating temperature for the two modes of operation, respectively.

The premium difference decreases as the evaporating temperature decreases; eventually becoming negative at the lower end of the temperature range. Since the premium difference is defined with respect to the cascade system, this indicates that the cascade system is more efficient when it

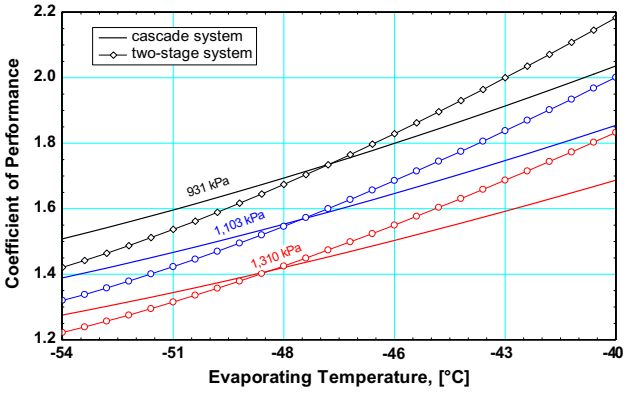

Fig. 5 – Optimized COP for both cascade system and two-stage systems as a function of evaporating temperatures over a range of system operating head pressures.

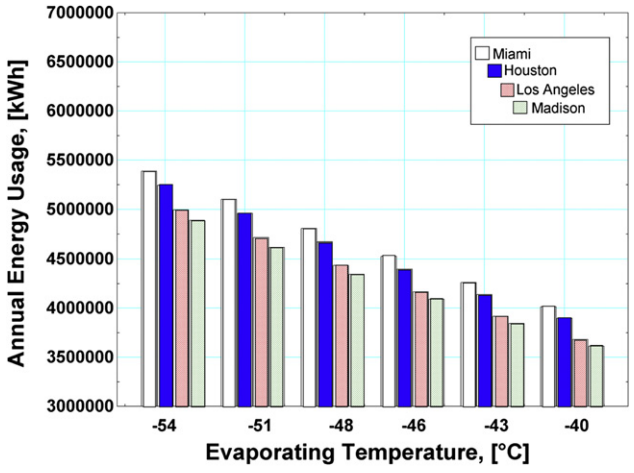

Fig. 6 – Annual energy usage for the cascade system operating in an 8-h day mode at various geographical locations as a function of evaporating temperature.

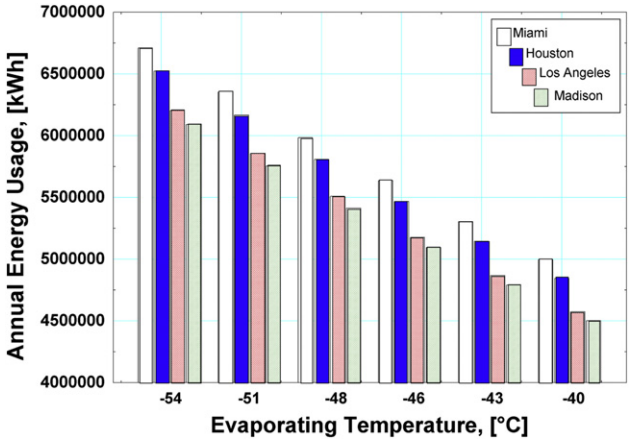

Fig. 7 – Annual energy usage for the cascade system operating in a 10-h day mode at various geographical locations as a function of evaporating temperature.

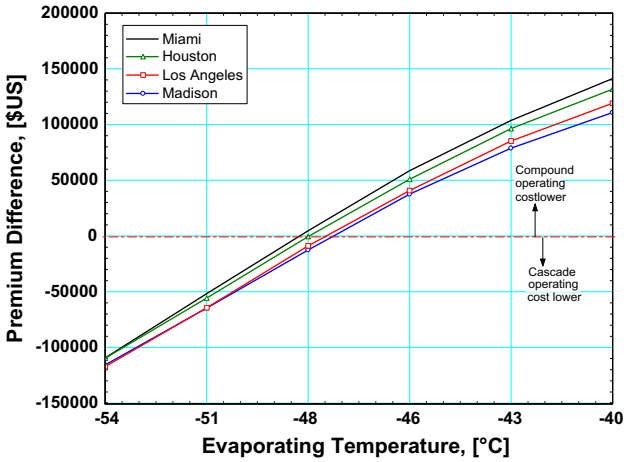

Fig. 9 – Premium difference between cascade system and two-stage system at various geographical locations for an 8-h day operating mode.

becomes negative. This trend is consistent with the *COP* results shown earlier. The two-stage system is more efficient at the higher end of the evaporating temperature range. The general trend is similar at each geographical location, but the magnitude of the premium difference varies. This behavior is attributed to the difference in average head pressure for each location. Since the change in head pressure has minimal effect on the premium difference, the rest of the economic study is conducted using a fixed representative head pressure of 1103 kPa.

9.3. *Capital cost savings*

For the purpose of evaluating the economic viability of the two systems, it is necessary to compare the difference in the capital cost associated with implementing their major components. Fig. 11 shows the adjusted capital cost (*ACC*) of the two cycles at the design operating conditions and a coincident system head pressure of 1103 kPa. The cascade system option includes costs for the low temperature circuit compressor, high temperature circuit compressor, and the cascade heat exchanger designed with an approach temperature of 5.6 K. The two-stage system cost includes the booster compressors, high-stage compressors and the intercooler. The adjusted capital cost comparison shows that the cascade system has an advantage of lower adjusted capital cost and this advantage increases as the evaporating temperature decreases. The increasing capital cost advantage for the cascade system option at lower evaporating temperatures is attributable to the rapid rise in compressor cost for the two-stage system due to the falloff in ammonia density at lower evaporating temperatures.

Fig. 12 shows the adjusted capital difference and the total life-cycle savings associated with selecting a two-stage system. The true break-even temperature associated with the cascade system with a 5.6 K cascade heat exchanger approach temperature is nominally −46.7 °C. It is

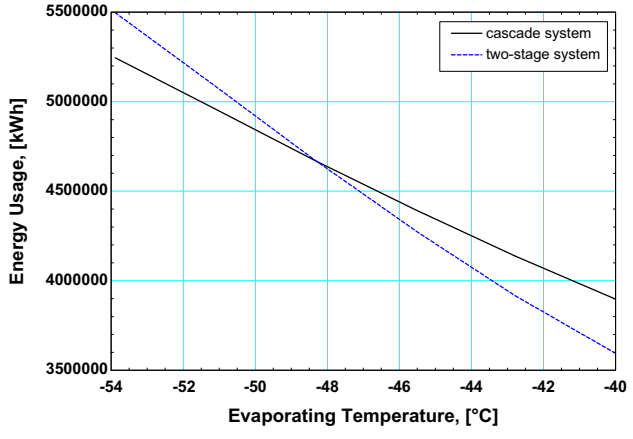

Fig. 8 – Annual energy usage for the cascade and two-stage systems as a function of evaporating temperatures operating at Houston, TX, for an 8-h day mode.

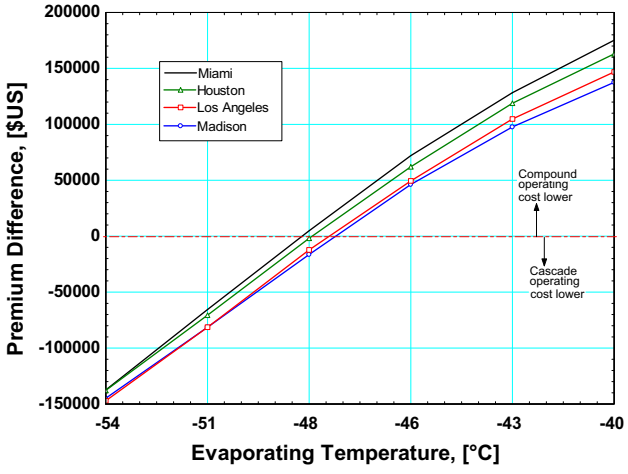

Fig. 10 – Premium difference between cascade system and two-stage system at various geographical locations for a 10-h day operating mode.

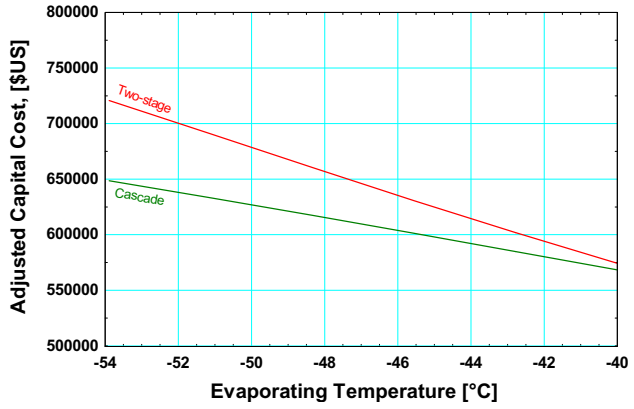

Fig. 11 – Adjusted capital cost of the cascade system and the two-stage system operating at 1103 kPa head pressure with a 5.6 K approach temperature.

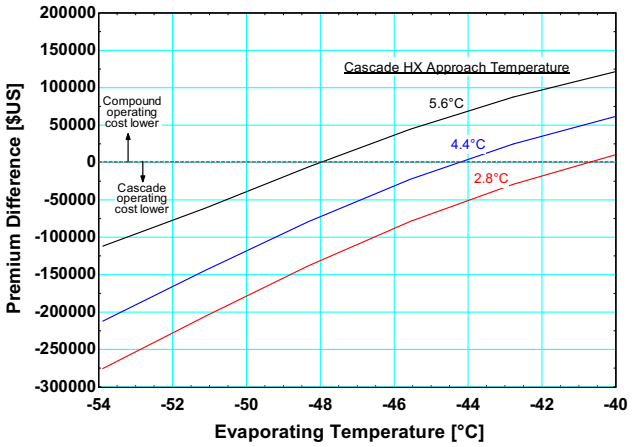

Fig. 13 – Premium difference between the cascade and two-stage systems over a range of evaporating temperatures for varying cascade heat exchanger approach temperatures (8-h day mode of operation).

important to note that the cost estimates indicated here do not reflect installed costs of total systems but the capital cost of only the major components that comprise each system.

There are many operating parameters that effect cascade system performance but the parameter that has the most significant impact on both the operating cost and the capital cost is the approach temperature. This parameter is studied in the subsequent section.

9.4. *Effect of approach temperature*

The cascade heat exchanger approach temperature significantly affects the economic analysis because the life-cycle cost of the cascade system depends on both the size (capital) and the performance (operating) of the CHE. Performance of the cascade system can be improved by selecting a larger CHE which allows a smaller approach temperature with a corresponding reduction in system operating costs; however, a larger CHE increases the capital cost of the cascade system. To assess the impact of CHE size, a sensitivity analysis is performed with the cascade approach temperature varying from 4.4 K (a 20% reduction from its nominal value of 5.6 K) and 2.8 K (a 50% reduction). The influence of the cascade approach temperature on the premium difference and the life-cycle savings is considered. Since head pressure has minimal effect on the premium difference, the results shown here are for a fixed head pressure of 1103 kPa.

Fig. 13 shows the premium difference between the two system configurations as a function of the saturated evaporating temperature with the cascade heat exchanger approach temperature as the parameter. Clearly, lower cascade heat exchanger approach temperatures offer the opportunity to greatly increase the operating efficiency of the cascade system option. Fig. 13 shows the break-even temperature (from an operating cost standpoint) shifting towards higher temperatures by nearly 3.9 K and 7.3 K when the approach temperature is reduced to 4.4 K and 2.8 K, respectively. The magnitude of the premium difference

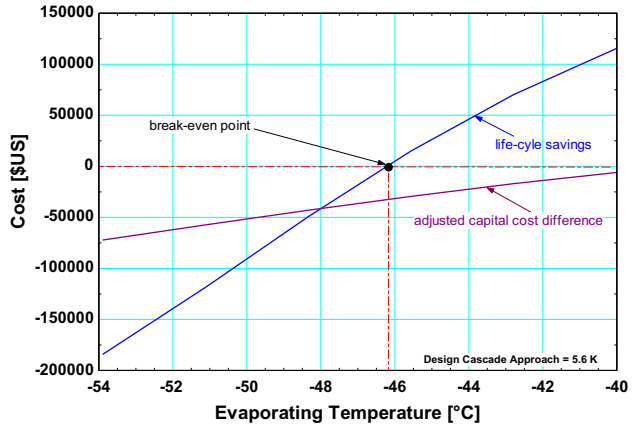

Fig. 12 – Comparative cost analysis for the cascade and two-stage systems operating at 1103 kPa head pressure with 5.6 K cascade heat exchanger approach temperature.

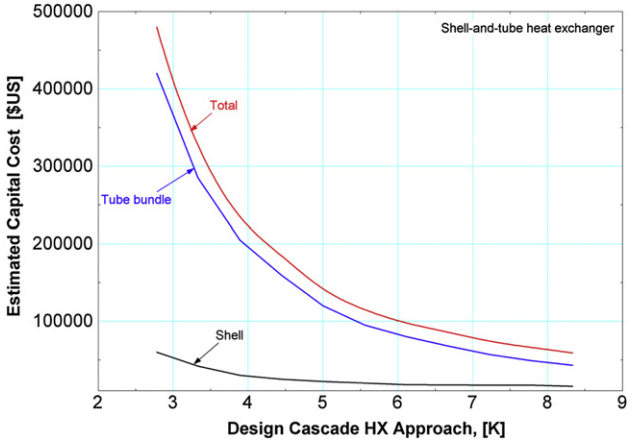

Fig. 14 – Estimated cascade heat exchanger capital cost as a function of cascade heat exchanger approach temperature.

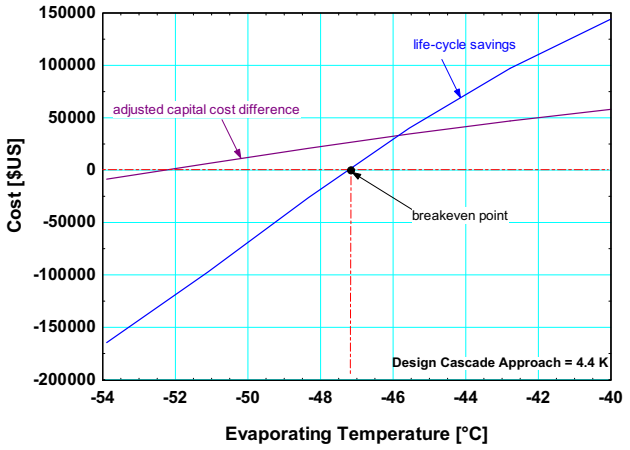

Fig. 15 – Comparative cost analysis for the cascade and two-stage systems operating at 1103 kPa head pressure with a 4.4 K design cascade heat exchanger approach temperature.

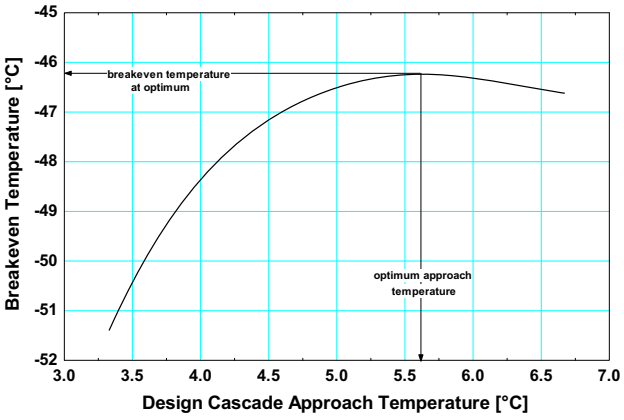

Fig. 17 – Break-even temperature of the cascade system and the two-stage system operating at 1103 kPa [160 psia] head pressure as a function of the design cascade condenser approach temperature.

also increases, towards the cascade system, substantially with the approach temperature reduction. Because the CHE capital cost is strongly affected by the approach temperature, smaller approach temperatures will lead to significantly higher CHE capital costs as shown in Fig. 14.

Fig. 15 illustrates the cost analysis results for a CHE approach temperature of 4.4 K. Because of the impact on the increased CHE cost to achieve a lower approach temperature, the break-even point for life-cycle savings shifts to a lower evaporating temperature compared to the base case approach temperature of 5.6 K shown in Fig. 12. Fig. 16 shows the cost results for a CHE approach temperature of 2.8 K. In this case, the adjusted capital cost difference increased dramatically and no break-even life-cycle savings was identified for the range of evaporating temperatures considered.

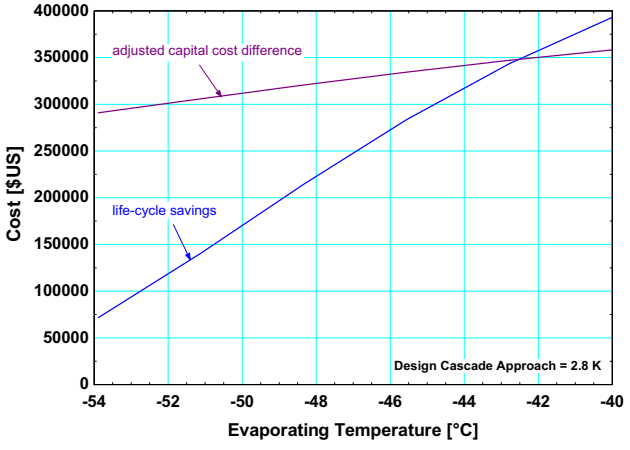

Fig. 16 – Comparative cost analysis for the cascade and two-stage systems operating at 1103 kPa head pressure with 2.8 K design cascade heat exchanger approach temperature.

9.5. *Optimal cascade heat exchanger approach temperature*

Previously, we showed that reducing the cascade approach temperature leads to an improvement in the premium difference for the cascade system but that effect is counteracted by a reduction in the adjusted capital cost difference which is driven by the increase of the cascade heat exchanger cost. It is of interest to understand how the cascade heat exchanger approach temperature influences the break-even temperature for the cascade system. A life-cycle saving analysis is carried out over a range of approach temperatures from 3.3 K to 6.7 K. Fig. 17 shows the results of this analysis for both the cascade and two-stage systems operating at a head pressure of 1103 kPa. The optimal design cascade approach temperature is 5.6 K and the corresponding break-even temperature is 46.2 °C. When the cascade system operates under this condition, the life-cycle savings is maximized and the range of evaporating temperatures that result in a life-cycle saving for the cascade system is the broadest, allowing the system to operate at higher evaporating temperatures while maintaining an economic advantage. Note that the break-even temperature changes most quickly between approach temperatures between 3.3 K and 3.9 K because, in this range, the cascade heat exchanger cost changes very quickly which outweighs the operating cost savings benefit of the cascade system. The results of this analysis suggests that a cascade system should be considered for applications in which the evaporating temperature will be less than −46.2 °C and that the cascade heat exchanger should be designed with an approach temperature difference of 5.6 K.

10. Conclusions

In this paper, we compare NH_3/CO_2 cascade system with a conventional two-stage ammonia system in order to determine the most attractive system configuration for a 2392 kW

thermal load application. The comparison is based on both system performance and economic viability. The intermediate condition for each cycle is optimized in order to maximize system efficiency (*COP*). The economics of the system is analyzed using the life-cycle cost analysis. The comparative energy and life-cycle economic analysis show that a cascade system is more efficient at low evaporating temperatures (below the break-even point) where energy usage is lower and the life-cycle cost savings is higher compared to the two-stage system. Reducing the cascade approach temperature increases cascade system COP and premium difference, but greatly increases the cascade system capital cost (due to the larger cascade heat exchanger that is required). An optimal cascade approach temperature of 5.6 K was found to provide the greatest life-cycle savings for the cascade system using a shell-and-tube cascade heat exchanger. The cascade system was found to be more economical than the two-stage system for applications that must operate below −46.2 °C.

REFERENCES

Ayub, Z.H., 2004. "Industrial refrigeration and ammonia enhanced heat transfer. In: Proc. of the ASME-ZSIS International Thermal Science Seminar II (CD-ROM), pp. 13–23. Slovenia.

Calm, J.M., Hourahan, G.C., 2007. Refrigerant data update. Heating/Piping/Air Conditioning Eng. 79 (No. 1), 50–64.

Cavallini, A., Censi, G., Del Col, D., Doretti, L., Longo, G.A., Rossetto, L., 2002. In-tube condensation of halogenated refrigerants. ASHRAE Trans.. paper H-1718.

Dopazo, A., Fernandez-Seara, J., Arias, A., Sieres, J., Uhia, F., 2007. "Thermodynamic analysis of a CO_2/NH_3 cascade refrigeration system", In: International Congress of Refrigeration. Beijing, China.

Evapco, 2005. ATC Evaporative Condensers. In: Product Bulletin, vol. 151-B. Evapco Inc. http://www.evapco.com.

Getu, H.M., Bansal, P.K., 2008. Thermodynamic analysis of an R744-R717 cascade refrigeration system. Int. J. Refrigeration 31, 45–54.

Grasso, 2008. Reciprocating Compressor Selection Program. Grasso Inc. under The GEA Group, Bochum, Germany.

Homsy, P., 2003. Ammonia/CO_2 Cascade System in a Large Freeze-drying Plant: Lessons Learned during Installation and Commissioning, Technical Paper #10, In: IIAR Ammonia Refrigeration Conference, Albuquerque, New Mexico, pp. 317–355.

Incropera, F., DeWitt, D., 2002. Fundamentals of Heat and Mass Transfer, fifth ed. John Wiley & Sons, New Jersey.

JCI, 2010. Compressor cost data obtained from both Frick Coolware 8.0 and personal communication with Johnson Controls Engineering personnel, Johnson Controls.

Lachner, B.F., 2004. The use of water as a refrigerant: impact of cycle modifications on commercial feasibility. M.S. Thesis, Mechanical Engineering, Solar Energy Laboratory, University of Wisconsin-Madison.

Lee, T.S., Liu, C.H., Chen, T.W., 2006. Thermodynamic analysis of optimal condensing temperature of cascade-condenser in CO_2/NH_3 cascade refrigeration systems. Int. J. Refrigeration 29, 1100–1108.

Manske, K.A., 1999. "Performance optimization of industrial refrigeration systems", M.S. Thesis, Mechanical Engineering, Solar Energy Laboratory, University of Wisconsin-Madison.

Mumanachit, P., 2009. "Comparative analysis of low temperature industrial refrigeration systems", M.S. Thesis, University of Wisconsin-Madison.

Nellis, Klein, 2009. Heat Transfer, first ed. Cambridge University Press, New York.

NREL, 2008. Typical Meteorological Year (TMY2) Weather Data. National Renewable Energy Laboratory. http://rredc.nrel.gov/solar/old_data/nsrdb/tmy2/.

Ouadha, A., Haddad, C., En-Nacer, M., Imine, O., 2007. "Performance comparison of cascade and two-stage refrigeration cycles using natural refrigerants", In: International Congress of Refrigeration, Beijing, China.

Page, A., 2002. CO2/NH3 refrigeration replaces R-22 in large freeze-drying plant. Technical Paper #1, In: IIAR Ammonia Refrigeration Conference, Kansas City, Missouri. pp. 1–27.

Pearson, A., 2005. Carbon dioxide-new uses for an old refrigerant. Int. J. Refrigeration, 1140–1148.

Pillis, J., 2009. "Energy consumption with CO_2/cascade systems", In: IIAR Industrial Refrigeration Conference & Exhibition. Dallas, Texas.

Taylor, C.R., 2002. Carbon dioxide-based refrigerant systems. ASHRAE J., 22–26.

UNEP, 2006. Report of the Refrigeration, Air conditioning, and Heat pumps Technical Options Committee (RTOC), United Nations Environment Programme. http://tiny.cc/vg4yc.